

Deletion of etoposide-induced 2.4 kb transcript (ei24) reduced cell proliferation and aggregate-size in *Dictyostelium discoideum*

NEHA GUPTA and SHWETA SARAN*

School of Life Sciences, Jawaharlal Nehru University, New Delhi, India

ABSTRACT The *etoposide-induced 2.4 kb transcript (ei24)* gene is induced both by p53 and etoposide, an anti-cancer tumour drug. There is no p53 gene present in *Dictyostelium discoideum*. Thus, the functions of *ei24* in the absence of p53 were analysed. Both overexpressor (*ei24^{OE}*) and knockout (*ei24*) mutants were made to study its role during growth, development and differentiation. Additionally, cell cycle and its response to DNA-damage were also analysed. We identified, characterized and elucidated the functions of the *ei24* gene in *Dictyostelium*. *In silico* analyses demonstrated the conservation across eukaryotes and *in situ* hybridization showed it to be prestalk-specific. *ei24* cells showed reduced cell proliferation and cell-cohesive properties, ultimately forming small-sized aggregates that developed into miniature and stalky fruiting bodies. The *ei24^{OE}* cells formed fruiting bodies with engorged or double-decker type sori with short stalks. The *ei24* cells showed reduced cAMP signalling with lower intracellular cAMP levels resulting in diminished migration of cells along cAMP gradients. Deletion of *ei24* resulted in mis-expression of prestalk-specific markers. Cell cycle analysis revealed an increased bias towards the stalk-pathway by *ei24* cells and vice-versa for *ei24^{OE}* cells. EI24 in *Dictyostelium* functions even in the absence of p53 and is induced in response to both UV-radiation and etoposide treatments. *ei24^{OE}* cells showed enhanced DNA-damage repair mechanisms. Also, etoposide treatment and overexpression of *ei24* caused G2/M arrest in the cell cycle. Our results indicate that EI24 is important for the growth, development and differentiation of *Dictyostelium* apart from being a DNA-damage response gene.

KEY WORDS: *Dictyostelium* EI24, cAMP signalling, etoposide, DNA-damage, cell cycle


Introduction

ei24 (*etoposide-induced 2.4 kb transcript*) also known as *PIG8* (*p53-induced gene 8*), encodes an ER-localized six transmembrane protein whose expression is highly induced by p53, a tumour-suppressor protein (Tian *et al.*, 2010). *ei24* is a DNA-damage response gene originally isolated from NIH-3T3 fibroblasts that were undergoing etoposide induced cell death (Gu *et al.*, 2000). Since there is an etoposide-induced apoptosis in a p53-dependent manner, it is considered to be a p53-regulated gene (Lehar *et al.*, 1996). Overexpression of *ei24* suppresses cell growth and induces apoptosis/autophagy while depletion results in suppression of apoptosis/autophagy in response to pro-apoptotic treatments (Zhao *et al.*, 2012). Essential role of EI24 has also been identified in early and late phases of autophagy in *C. elegans*

and humans (Tian *et al.*, 2010). Recently, it has been postulated that autophagic degradation of RING E3 ligases is also mediated through EI24, thus establishing a connection between autophagy and the ubiquitin-proteasome system (Devkota *et al.*, 2016) and proposed as autophagy-UPS crosstalk. The physiological functions of EI24 are still poorly understood.

Etoposide is a chemotherapeutic agent that induces DNA double-stranded breaks (DSBs) by inhibiting DNA topoisomerase II enzymes (Yang *et al.*, 2009). Many genes that are activated in response to DNA-damaging agents are also under the control of cell cycle (Dasika *et al.*, 1999). It is thus critical that DNA-DSBs are detected, signalled and repaired in order to maintain genome

Abbreviations used in this paper: Dd, *Dictyostelium discoideum*; ei24, etoposide-induced 2.4 kb transcript; ER, endoplasmic reticulum.

*Address correspondence to: Shweta Saran. School of Life Sciences, Jawaharlal Nehru University, New Delhi-110067, India. Tel: (O) +91-11-26704157. E-mail: ssaran@mail.jnu.ac.in; shweta_saran@hotmail.com -  <http://orcid.org/0000-0002-0238-498X>

Supplementary Material (three videos, five figures and one table) for this paper is available at: <http://dx.doi.org/10.1387/ijdb.170327ss>

Submitted: 23 November, 2017; Accepted: 13 February, 2018.

integrity. Activation of specific genes is a primary response by cells to the damaged DNA (Albrechtsen *et al.*, 1999). In case of *Dictyostelium*, both homologous recombination (HR) and non-homologous end-joining (NHEJ) pathways are operational during the vegetative stage and the importance of Ku and PKCs in regulating DSB repair has been established (Hsu *et al.*, 2011).

Here, we illustrate the functions of *Dictyostelium discoideum* *ei24*. *Dictyostelium*, a protist undergoes both vegetative growth (unicellular amoebae) and development (multicellular) that are mutually independent of each other. The amoebae grow and divide mitotically till food is sufficient but upon starvation, the isolated amoebae come towards common collecting points to form multicellular structures. Movement and organization of cells during development is largely dependent on cAMP signalling (Jang *et al.*, 2002). The sizes of the aggregates formed depend on cAMP signalling, cell-adhesion molecules and other factors that help to sense cell density (Jang and Gomer, 2008). It was earlier observed that *smIA* mutants formed small-sized aggregates due to over-secretion of CountinA protein (Brock and Gomer, 1999). The migrating slug formed from the aggregate have prestalk cells in the anterior and prespore cells in the posterior. Interestingly, the ratio of cell-types remains constant and independent of the size of the multicellular structures formed. The prestalk region is further divided into subtypes: *pstA* occupy the anterior 10% of the slug, *pstAB* cells occupy the core of the tip and the *pstO* are

found behind the *pstA* region. The anterior-like cells (ALCs) are randomly distributed in the prespore region (Early *et al.*, 1993). Eventually, a fruiting body is formed that is composed of two terminally differentiated cells: the spores (viable) and the stalk (dead, vacuolated) (Whittingham and Raper, 1960). Thus, many genes play a role in maintaining the cell-type proportioning and patterning (Balint-Kurti *et al.*, 1997; Ginsburg and Kimmel, 1997; Chung *et al.*, 1998; Han and Firtel, 1998).

Functions of *ei24* during the development of *Dictyostelium* were characterized with the help of mutants, [overexpressor (*ei24^{OE}*) and knockout (*ei24⁻*)] created during this study. *ei24⁻* cells showed reduced cell proliferation and delayed development forming stalky fruiting bodies with decreased spore-viability and abridged cAMP signalling when compared to wild type and *ei24^{OE}* strains. We show, *EI24* plays a regulatory role in the spatial cell-type patterning as the mutation caused mis-localization of prestalk cells and a decrease in prespore cells, ultimately resulting in fruiting bodies with small sori and long stalks. We also observed increased *ei24* mRNA expression upon treatment with two DNA damaging agents- etoposide and UV-C radiation. The levels of DSB repair genes were elevated in response to etoposide treatment or upon *ei24* overexpression and the cell cycle analysis showed G2/M arrest upon similar treatments. The *ei24* expression was independent of *Dictyostelium* DDB_G0288895 gene, which is referenced as *p53-like* in dictyBase. To conclude, *ei24* is an *etoposide-induced*

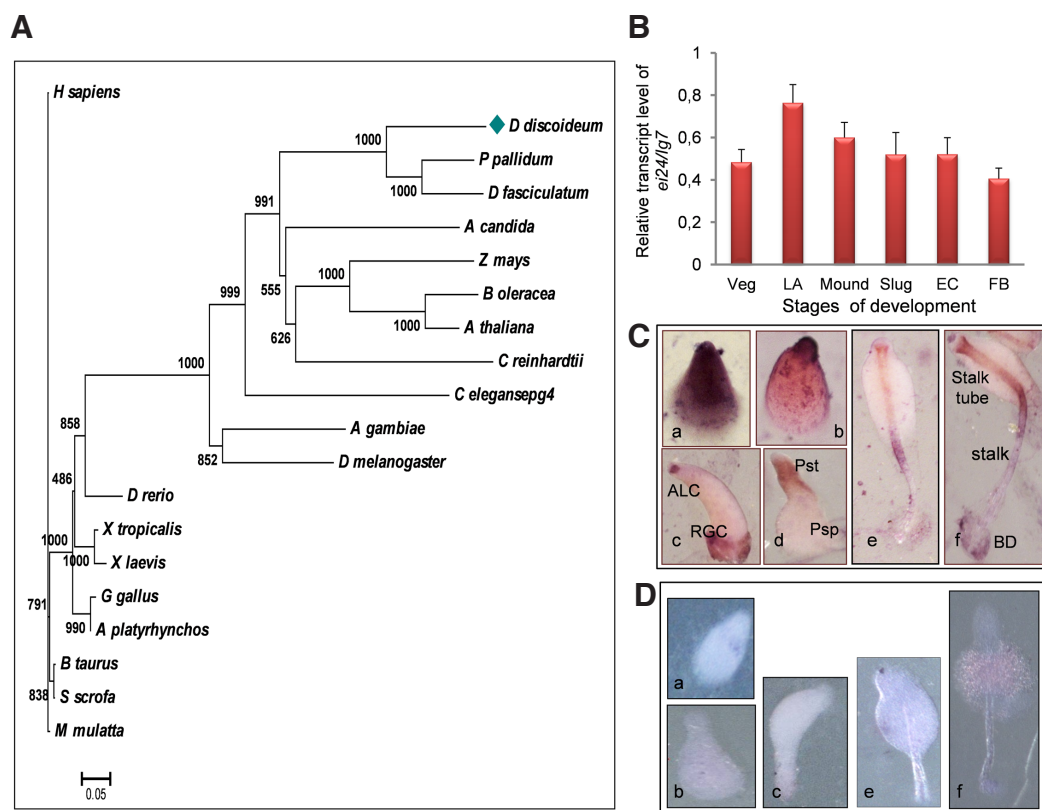


Fig. 1. *Dictyostelium* EI24 shows homologs in other organisms and is enriched in prestalk/stalk cells.

(A) A CLUSTALX alignment of *EI24* full-length protein sequences from different organisms was used to create a bootstrap neighbour-joining (N-J) tree. The tree was rooted on the human *EI24*. Bootstrap values are provided at the node of each branch. The scale bar indicates amino acid substitutions per site. *H sapiens*, Homo sapiens (AAC39531.2); *D discoideum*, *Dictyostelium discoideum* (XP_638676.1); *P pallidum*, *Polysphondylium pallidum* (XP_020436505.1); *D fasciculatum*, *Dictyostelium fasciculatum* (XP_004350815.1); *A candida*, *Albugo candida* (CC147573.1); *Z mays*, *Zea mays* (ONM17391.1); *B oleracea*, *Brassica oleracea* (XP_013606043.1); *A thaliana*, *Arabidopsis thaliana* (NP_849325.4); *C reinhardtii*, *Chlamydomonas reinhardtii* (XP_001690067.1); *C elegans*, *Caenorhabditis elegans* (NP_498575.1); *A gambiae*, *Anopheles gambiae* (XP_317350.4); *D melanogaster*, *Drosophila melanogaster* (NP_608864.1); *D rerio*, *Danio rerio* (NP_001017898.1);

X tropicalis, *Xenopus tropicalis* (NP_001017187.1); *X laevis*, *Xenopus laevis* (NP_001088433.1); *G gallus*, *Gallus gallus* (CAG31919.1); *A platyrhynchos*, *Anas platyrhynchos* (XP_012955067.1); *B taurus*, *Bos taurus* (CUA68216.1); *S scrofa*, *Sus scrofa* (XP_003130093.1); *M mulatta*, *Macaca mulatta* (NP_001244437.1). **(B)** Relative *ei24* mRNA expression during growth and development of *D. discoideum*. *ig7* was used as an internal control. **(C)** In situ hybridization using antisense strand shows the presence of *ei24* mRNA largely in the prestalk/stalk cells of multicellular structures developed. **(D)** In situ hybridization using sense strand represents the negative control. [*n*=3; Veg-vegetative, LA-loose aggregate, EC-early culminant, FB-fruiting body, RGC-rear-guard cells, ALC-anterior-like cells, *pst*-prestalk, *psp*-prespore, BD-basal disc; a-LA, b-Mound, c,d-slug, e-EC, f-late culminant/FB].

gene, involved in growth and development of *Dictyostelium* and is a DNA-damage response gene.

Results

The *D. discoideum* genome encodes one *ei24* gene

D. discoideum EI24 family protein (*DdEI24*; Gene ID: *DDB_G0284253*) codes for a putative transmembrane protein and showed 26% identity to human EI24. Phylogenetic analyses showed *DdEI24* to be evolutionarily closer to the proteins of plants rather than animals (Fig. 1A). Homologs are present in *Arabidopsis thaliana*, *Caenorhabditis elegans* and *Drosophila melanogaster* but not in *Saccharomyces cerevisiae*. *Ddei24* gene encodes a 307 amino acid long protein with a predicted molecular mass of 35.9 kDa and has six putative transmembrane domains. The potential topology motifs as detected by the PSORT II program show ER membrane retention signal (TTKQ) at the C-terminus suggesting it to be located in the membrane-spanning regions (electronic supplementary material, Fig. S1).

ei24 mRNA is expressed in prestalk/stalk cells

The spatiotemporal mRNA expression patterns of *ei24* were determined by reverse transcriptase PCR (RT-PCR) and *in situ* hybridization analyses. *ei24* mRNA was present throughout growth and development. The level was low in the vegetative cells and was highest during aggregation. Thereafter, a gradual decrease till fruiting body formation was observed (Fig. 1B).

Whole mount *in situ* hybridization analysis showed *ei24* transcript in the tight aggregates (Fig. 1Ca). As they proceed into development, the transcript was restricted to the prestalk, the rear-guard and the anterior-like cells (Fig. 1Cb-d). During culmination, the transcript was exclusively in the stalk tube, stalk and the basal disc region (Fig. 1Ce, f). The results obtained with sense probe did not show any specific staining (Fig. 1D). In conclusion,

the *ei24* transcript showed prestalk/stalk localization and was present throughout growth and development.

DdEI24 fusion protein is localized in the endoplasmic reticulum

To analyse the biological functions of *ei24*, we generated *ei24* strain in Ax2 cells by homologous recombination using *Bsr* cassette. Upon transformation, cells were selected with 10 $\mu\text{g ml}^{-1}$ Blasticidin S and 500 independent clones were screened for the presence of positional integrants through various PCR amplifications of the genomic DNA (electronic supplementary material, Fig. S2). Out of the two positional integrants representing *ei24* null mutant (*ei24*⁻), one of them was used for further studies and examined for the deletion effect. Vegetative cells from each of the mutant strains along with Ax2 were collected and cDNA was prepared to measure the mRNA levels of *ei24*. Expression of *ei24* increased by ~3-4 folds in case of *ei24*^{OE} as compared to Ax2 while in *ei24*^{Res}, the levels were similar to that in the wild type. We could not detect any significant levels of *ei24* in the knockout strain (Fig. 2A).

Due to the unavailability of antibody specific to *Dictyostelium* EI24, we could not assess its abundance and localization in *D. discoideum*. Thus, we localized the EI24 fusion protein in the *ei24*^{OE} strain. The eYFP fluorescence of the EI24-eYFP fusion protein in growing cells as revealed by confocal microscopy was observed as a network throughout the cytoplasm and around the nucleus (Fig. 2B upper panel). This network co-localized largely with the ER-Tracker Red (ThermoFisher Scientific) fluorescence, a marker for ER. Co-localization was quantitated through coloc2 plugin using ImageJ software, where the Pearson's R value was found to be 0.64 ± 0.1 , thus confirming the colocalization of the EI24 fusion protein with ER (Fig. 2B, middle panel; electronic supplementary material, Fig. S3). EI24-eYFP fluorescence did not co-localize with the Mito-tracker red (Sigma Aldrich) (Fig. 2B, lower panel), a marker for the mitochondria.

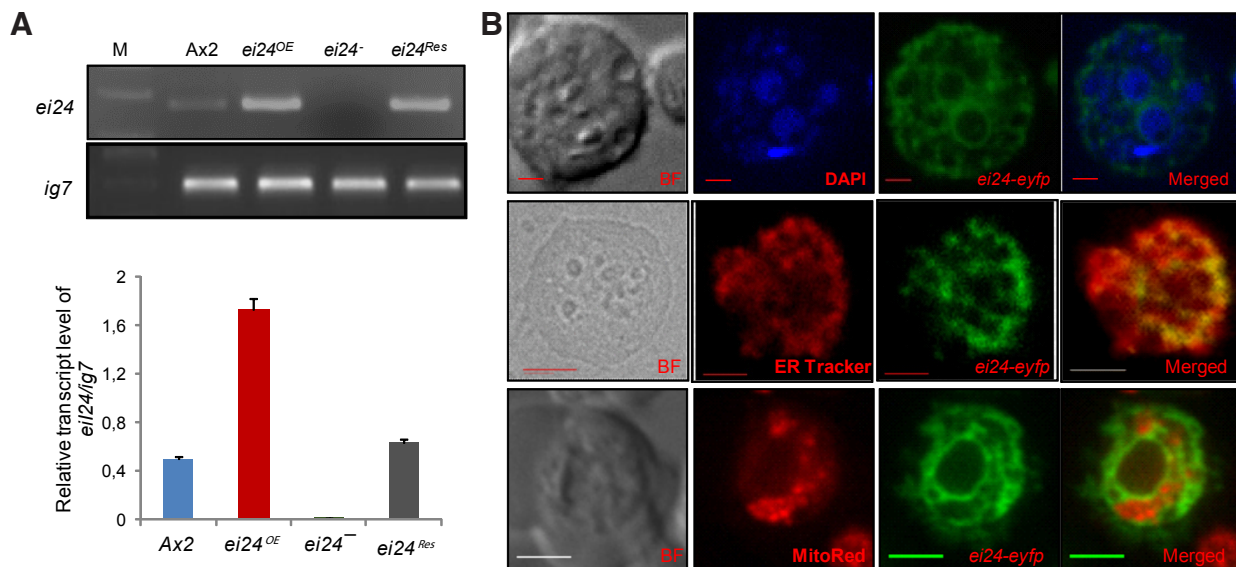


Fig. 2. Expression of *ei24* in the mutants and the recombinant fusion protein (EI24-eYFP) interspersed with membranous regions spanning the endoplasmic reticulum (ER). (A) Confirmation of strains by determining the mRNA expression of *ei24* in the vegetative cells of Ax2, *ei24*^{OE}, *ei24*⁻ and *ei24*^{Res}. Upper panel: one representative gel picture; lower panel: a graphical representation of the same ($n=3$). (B) Upper panel: Nuclear stain with DAPI (blue) and green fluorescence due to the fusion protein. Middle panel: Red due to ER-tracker dye and green due to fusion protein. Co-localization can be observed. Lower panel: Red due to MitoRed dye and green due to fusion protein. No overlap was observed. [Scale bar, 10 μm ; BF, brightfield].

DdEi24 is required for normal cell proliferation and development

To measure the rate of cell proliferation in liquid culture, Ax2, *ei24^{OE}*, *ei24⁻* and *ei24^{Res}* log phase cells were identically inoculated at a cell density of 5×10^5 cells ml⁻¹ in fresh HL5 medium and monitored for several days. All the strains reached their maximum density at the same time (t72). Both, Ax2 and eYFP/Ax2 cells reached the stationary phase at a density of approximately $1.2 \pm 0.19 \times 10^7$ and $1.19 \pm 0.12 \times 10^7$ cells ml⁻¹, respectively; the *ei24⁻* cells reached at a density of $0.69 \pm 0.09 \times 10^7$ cells ml⁻¹; the *ei24^{OE}* cells reached at a density of $1.35 \pm 0.12 \times 10^7$ cells ml⁻¹ and the *ei24^{Res}* cells reached at a density of $1.2 \pm 0.13 \times 10^7$ cells ml⁻¹. We observed decreased cell proliferation in *ei24⁻* cells as compared to the wild type cells in liquid culture. Ax2 cells overexpressing *ei24* exhibited slightly higher proliferation rate as compared to the wild type. Reintroduction of *ei24:eYFP* into *ei24⁻* cells (*ei24^{Res}*) could restore normal growth confirming the phenotype was indeed due to the deletion of *ei24* (Fig. 3A). The doubling time for Ax2, *ei24^{OE}*, *ei24⁻*, *ei24^{Res}* were 11.08 ± 0.27 , 9.21 ± 0.52 , 25.25 ± 0.51 and 14.98 ± 0.59 h, respectively.

To examine the role of *ei24* in development, the *ei24* mutant strains along with wild type controls were developed on NNA plates at a medium density of 3×10^5 cell cm⁻² (Fig. 3B). Nearly 40% of the fruiting bodies formed from *ei24^{OE}* cells showed double-decker type sori while rest of them had comparatively larger sori (Fig. 3B, lower panel). Deletion of *ei24* caused the formation of fruiting bodies with longer stalks and smaller sori while overexpression caused the fruiting bodies to have larger sori and shorter stalks (Figs. 3B, lower panel; 4C). The numbers of aggregates formed were significantly higher but undersized in *ei24⁻* cells and showed a delay in development forming fruiting bodies by 30 h after starvation as compared to the wild type, which took nearly 24 h. On the other hand, *ei24^{OE}* cells formed larger but fewer aggregates,

which formed fruiting bodies by 24 h after starvation (Fig. 4A, B). Even, the numbers of spores formed by *ei24⁻* cells were fewer and showed lesser viability as compared to the wild type. The number of spores by *ei24^{OE}* cells was significantly higher than the wild type and showed higher viability (Fig. 4D, E). The number of spores encapsulated in each sorus varied to the same extent as the size of sorus *i.e.* *ei24⁻* strain produced very few spores with reduced spore-viability suggesting an important role for EI24 in development and spore differentiation.

ei24⁻ cells show reduced cAMP signalling

Since, cAMP levels and the cell-adhesion molecules play an important role in determining the time and size of the aggregates formed, we checked for them in the mutant cells and compared them to the wild type. cAMP levels under starved conditions were almost double in case of *ei24^{OE}* cells while the *ei24⁻* cells showed lower cAMP levels as compared to Ax2 cells (Fig. 5A). Increased cAMP levels may account for the larger aggregate-size. Cell-cohesion also contributes towards aggregate-size and our results showed that the *ei24⁻* cells had lower while the *ei24^{OE}* cells had higher cohesive properties as compared to the wild type cells (Fig. 5B).

To substantiate the movement of cells in response to extracellular cAMP, cell migration assay was performed, which showed significantly higher chemotactic migration towards the gradient of cAMP by the *ei24^{OE}* cells while *ei24⁻* cells showed nearly 50% lower levels than the wild type cells (Fig. 5C; supplementary videos V1-V3).

Since the effective cAMP levels in the null cells were reduced, we observed small-sized aggregates as well as reduced spore-viability. We thus analyzed the individual components involved in the initial cAMP signal transduction pathway like *acaA* (adenylyl cyclase A), *carA1* (cyclic AMP receptor 1), *gbfA* (G-box binding factor) and *pdsA* (extracellular cAMP phosphodiesterase). We

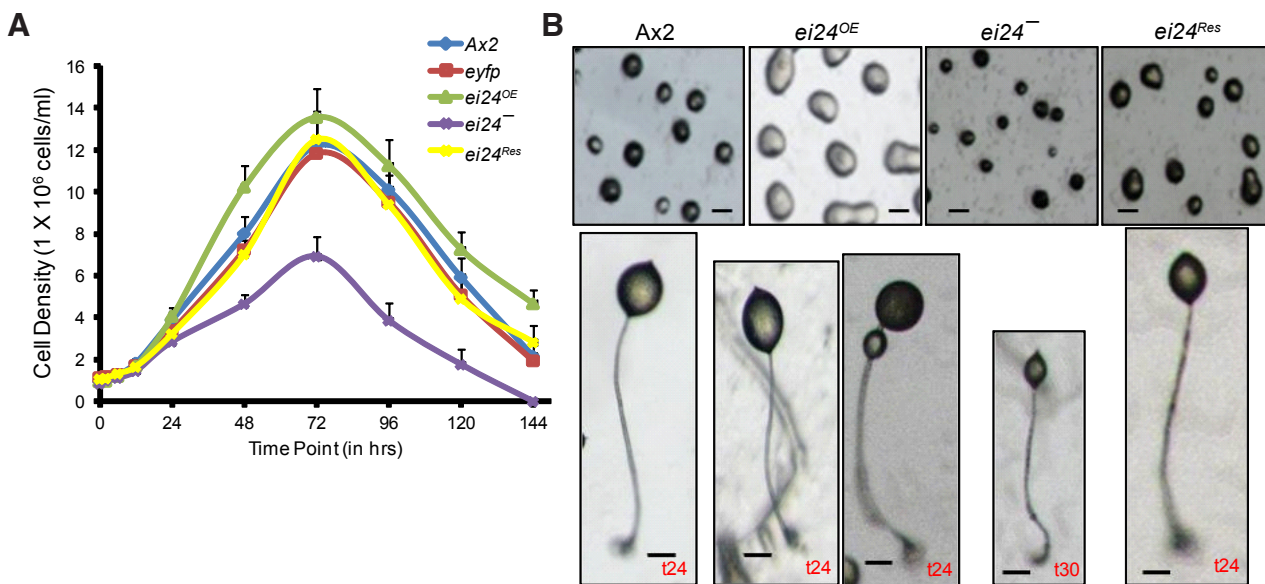


Fig. 3. *ei24* mutants cause aberrant growth and development. (A) Graph represents growth profile of the mutants (*ei24^{OE}* and *ei24⁻*), wild type (Ax2 and eYFP/Ax2) and rescue (*ei24^{Res}*) strains. The *ei24⁻* cells showed slow cell proliferation. (B) Images showing development profile of Ax2, *ei24^{OE}*, *ei24⁻* and *ei24^{Res}* strains. Upper panel: aggregate of the foresaid strains; lower panel: the fruiting body of the same (development time is mentioned). The *ei24⁻* cells showed a delay in development and formed fruiting body with a long stalk and small sorus. The *ei24^{OE}* showed normal developmental time and formed fruiting body with a large sorus and small stalk. (Number of structures analysed ~ 200; n=3; scale bar, 100 μ m).

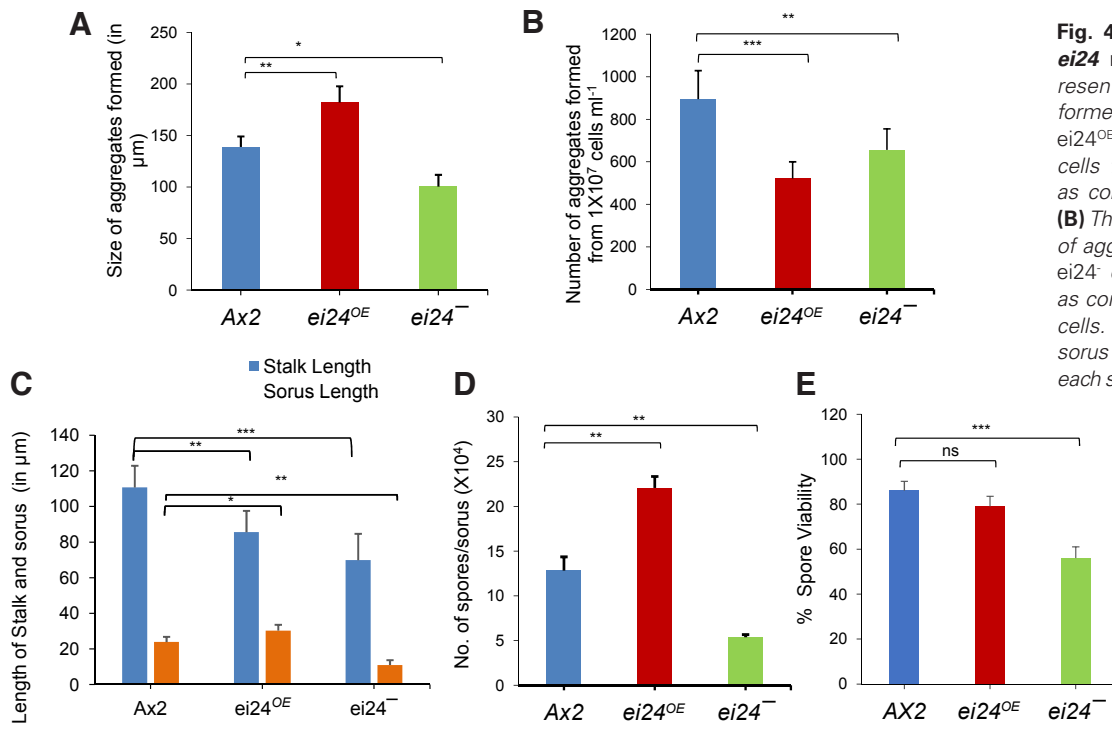


Fig. 4. Morphological analyses of *ei24* null cells. (A) The graph represents the size of aggregates (μm) formed by Ax2, *ei24^{OE}* and *ei24⁻* strains. *ei24^{OE}* cells formed large while *ei24⁻* cells formed small sized-aggregates as compared to the wild type cells. (B) The graph represents the number of aggregates formed by each strain. *ei24⁻* cells formed fewer aggregates as compared to *ei24^{OE}* and wild type cells. (C) Panel represents the stalk: sorus ratio of fruiting bodies formed by each strain. *ei24^{OE}* formed spory while *ei24⁻* forms stalky fruiting bodies. (D) Graph represents the average number of spores per sorus. (E) Graph represents reduced spore-viability upon deletion of *ei24*. [The values representing mean \pm standard error (S.E.); number of structures analysed ~ 200 ; $n = 3$; Student *t*-test, p -value ≤ 0.05 , ≤ 0.01 and ≤ 0.001 has been represented as *, ** and ***, respectively].

observed a decrease in *acaA* and *carA1* levels during development of *ei24⁻* cells. The phosphodiesterase, *pdsA* during early development was decreased but thereafter-showed comparable levels. The *gbfA* whose expression is dependent on cAMP levels was reduced (Fig. 6A-D). Taken together, the results suggested a decrease in the components controlling cAMP levels, which confirms our earlier observations. The cAMP levels were decreased but not abolished as these cells do complete development. The cell-adhesion proteins play an important role in group-size determination thus, the two cell-adhesion proteins Gp24 (CadA) and Gp80 (CsA) that are expressed during early developmental stages were also monitored. The mRNA level of *cadA* was significantly increased in the *ei24⁻* cells resulting in increased cell-adhesive properties and *csA*, that is required to break the aggregation stream

was significantly reduced (Fig. 6E, F). mRNA levels of the Countin protein that is required for the break-up of streams, was higher in case of null cells (Fig. 6G). Reduced mRNA levels of the spore coat proteins; CotA and CotB confirmed the stalky phenotypes and reduced spore-viability observed in *ei24⁻* cells (Fig. 6H, I).

Taken together our results show reduced cAMP levels, small-sized aggregates, feeble chemotaxis and reduced spore-viability by the *ei24⁻* cells.

Prestalk-specific markers were mis-expressed in *ei24⁻* cells

Since the *ei24⁻* cells formed aberrant phenotype, we were interested in elucidating the role of EI24 in regulating cell-type patterning. For this, we measured the mRNA levels of the cell-type specific marker genes during development of both Ax2 and

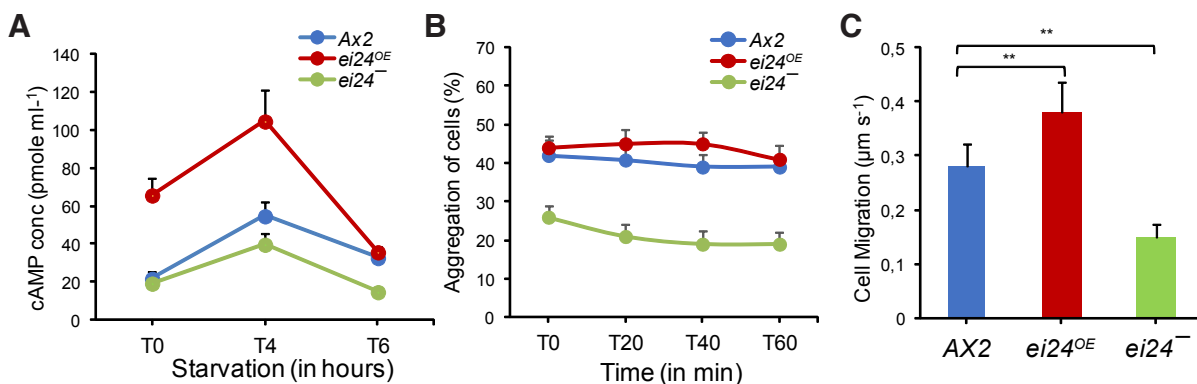


Fig. 5. *ei24^{OE}* cells formed large-sized aggregates due to high cAMP levels and increased cohesive properties. (A) Graph shows intracellular cAMP levels in various strains. cAMP concentrations in *ei24⁻* cells upon starvation was reduced while the levels were increased in the *ei24^{OE}* cells. (B) Graph representing reduced percentage of aggregating cells in the *ei24⁻* cells. (C) Bar diagram represents cell migration (in $\mu\text{m s}^{-1}$). *ei24⁻* cells show reduced and *ei24^{OE}* cells show increased cell migration when compared to the wild type cells. [The values representing mean \pm S.E.; $n=3-5$; cells analysed for migration = 100 for each strain; Student *t*-test, p -value ≤ 0.01 has been represented **].

ei24 cells. Expression of prestalk-specific genes, like *ecmA* and *ecmB*, were significantly increased in the *ei24* cells. Also, the level of *pspA* (*d19*), a prespore marker gene expression was reduced during development when compared to the wild type cells (electronic supplementary material, Fig. S4). We believed this to be the possible reason for the aberrant phenotype observed by the *ei24* cells. We thus substantiated our results by examining the spatial cell-type patterning using cell-type specific promoters fused to *lacZ* reporter in both Ax2 and *ei24* cells. Our results showed increased staining area and mis-localization of prestalk-specific markers while there was reduced staining of the *pspA* gene in the multicellular structures studied (Fig. 7).

We compared the spatial distribution of the prestalk- and prespore-specific markers in various structures formed by Ax2 and *ei24* cells. The expression of *ecmA* was distributed throughout the mound formed by the *ei24* cells (Fig. 7Aa,a'). The first finger, migrating slugs, early culminants formed, also showed extended staining in the prestalk regions, ALCs and the RGCs (Fig. 7Ab,b', c,c', d,d'). The *lacZ* staining regions of *ecmB*, *ecmO* and *ecmA*O observed in the multicellular structures developed by the *ei24* cells were observed to be more as compared to the Ax2 cells.

The *ecmB* expression was high in the prestalk region but not in the most anterior-tip region of the structures formed. There was immense staining observed in the ALCs, basal disc, upper and lower cups and the stalk tube (Fig. 7Ba-e'). *ecmO* staining was also extended to the ALCs, RGCs, stalk, basal disc and also covered the entire prestalk region of the structures formed (Fig. 7Ca-e'). The staining pattern observed for *ecmA*O was higher at all stages of development. Interestingly, there was more staining in the ALCs (Fig. 7Da-e'). On the other hand, the *lacZ* staining pattern of the *pspA* was reduced in all the structures formed by the *ei24* cells as compared to the Ax2 cells (Fig. 7Ea-e') except in the fruiting bodies formed. We observed more staining in the stalk and basal disc regions of the fruiting body formed by the *ei24* cells as compared to that of Ax2.

To wrap up the results, it is postulated that *ei24* cells showed enhanced prestalk cell-type patterning, which ultimately resulted in stalky fruiting bodies with a reduced prespore region.

***Ddei24* is p53-like independent and is induced by etoposide**

In *D. discoideum*, we could not find any *p53* gene but a *p53*-like gene (*DDB_G0288895*) has been identified in dictyBase, which did

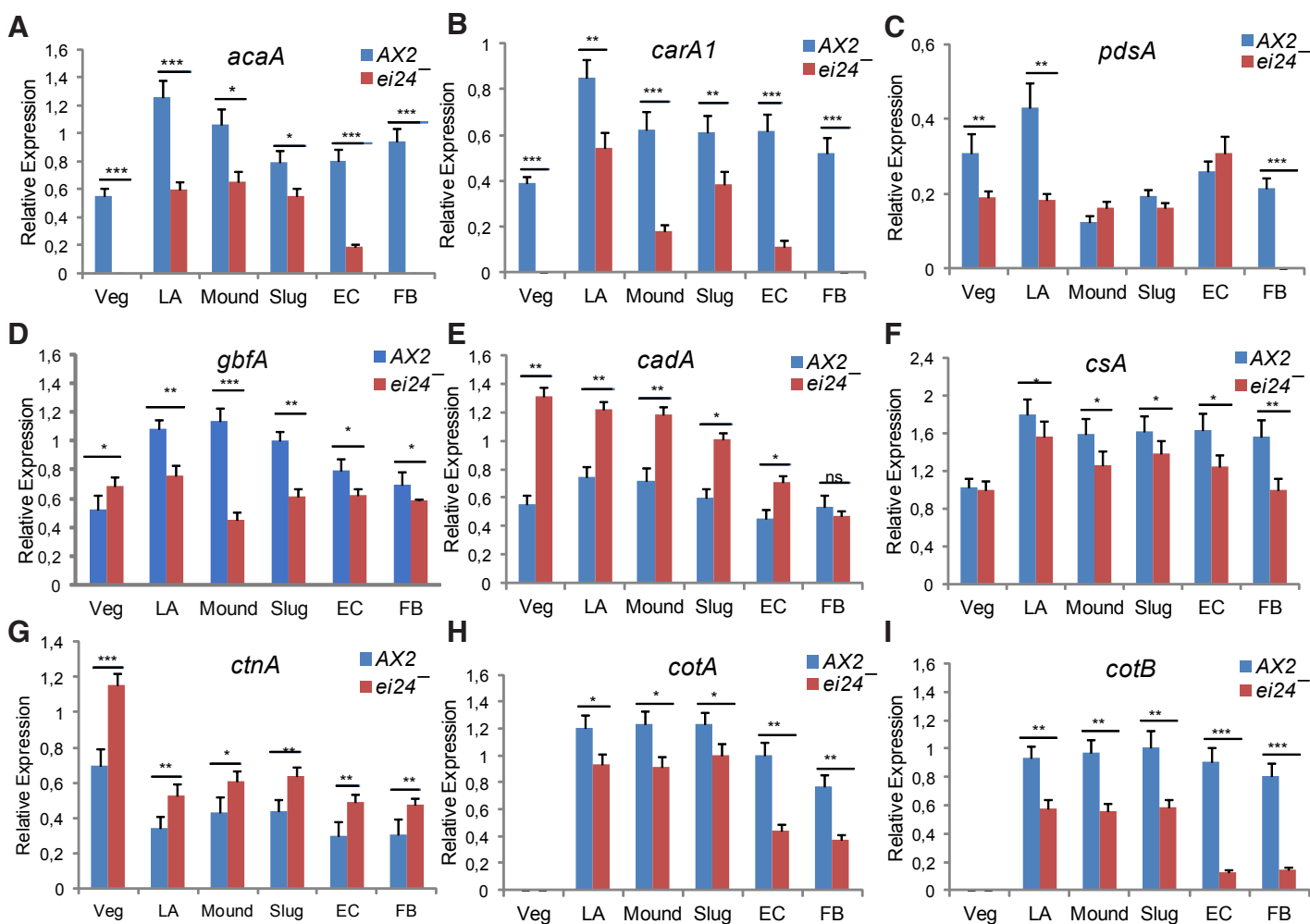


Fig. 6. *ei24* cells showed altered mRNA expression of genes involved in development. RT-PCR analyses of specific genes (A) *acaA*, (B) *carA1*, (C) *pdsA*, (D) *gbfa*, (E) *cadA*, (F) *csaA*, (G) *ctnA*, (H) *cotA* and (I) *cotB* during development of Ax2 and *ei24*⁻ after normalization to *ig7* are shown. [Veg, vegetative; LA, loose aggregate; EC, early culminant; FB, fruiting body. *n*=3; Student *t*-test, *p*-value ≤ 0.05 , ≤ 0.01 and ≤ 0.001 has been represented as *, **, and ***, respectively].

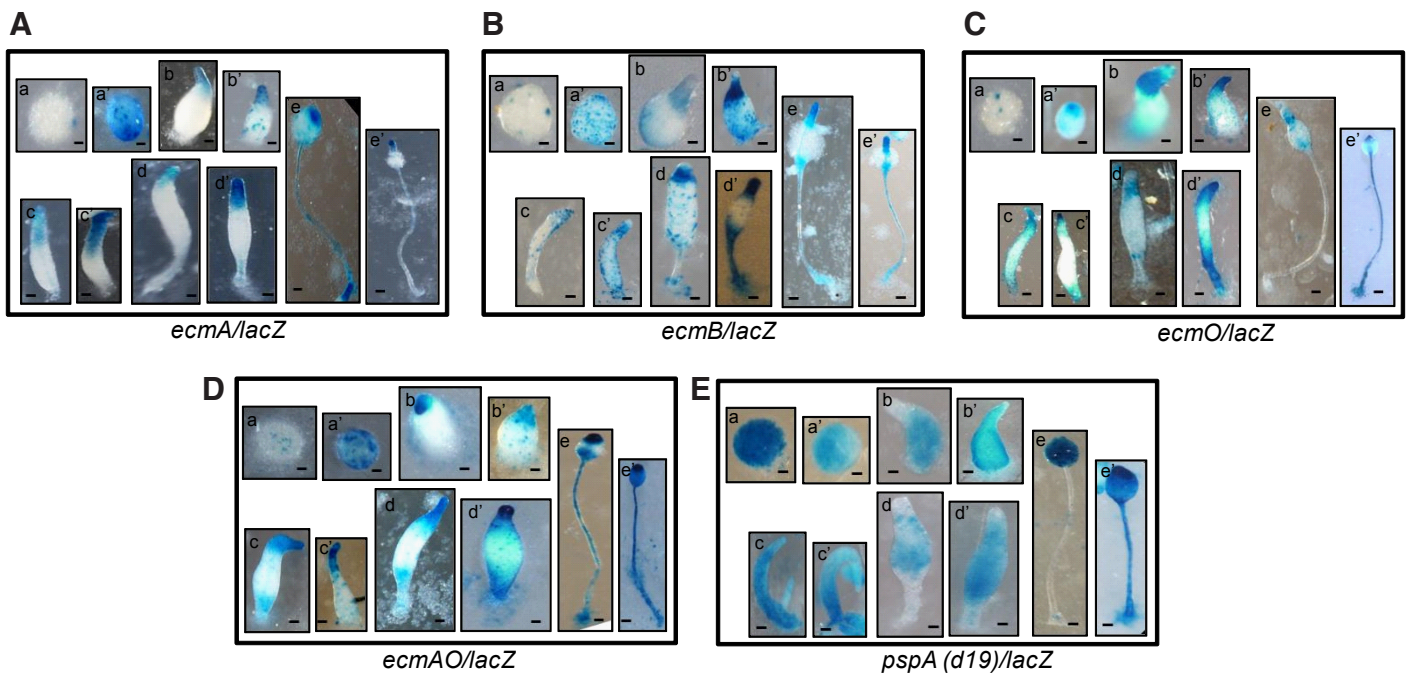


Fig. 7. *ei24* cells showed altered expression of cell-type specific genes. *Ax2* and *ei24*- cells were transformed with prestalk-specific marker genes like (A) *ecmA*, (B) *ecmB*, (C) *ecmO*, (D) *ecmAO* and prespore-specific gene, (E) *pspA* (d19). Cells were developed on nitrocellulose filters and histochemical X-gal staining was performed to visualize the specific staining patterns in multicellular structures. [In each panel a,a', aggregate; b,b', tipped mound; c,c', slug; d,d', early culminant; e,e', late culminant of *Ax2* and *ei24* strains, respectively. Scale bar represents 50 μm ; $n = 3$; structures analyzed per strain = 100].

not show any similarity to human *p53* and also lacked any specific *p53* domain (data not shown). Presently, we show the expression pattern of *DDB_G0288895* remained unchanged in *ei24* mutant strains and also, the expression pattern of *ei24* was not affected by overexpression of *DDB_G0288895* (Fig. 8A). We conclude, that *DDB_G0288895* is either wrongly annotated in dictyBase as *p53*-like gene or alternatively, *EI24* functions independent of it. Increased *ei24* expression was observed upon UV-C irradiation both in terms of mean intensity of eYFP fluorescence as well as mRNA expression (Fig. 8B). Wild type and *ei24* mutant cells when treated with different doses of etoposide, showed induction of *ei24* mRNA in *Ax2* cells but not in *ei24^{OE}* and *ei24⁻* cells (Fig. 8C). The maximum expression was observed at 40 $\mu\text{g ml}^{-1}$ of etoposide treatment. MTT assay confirmed our results showing *ei24⁻* cells were protected from etoposide-induced cell death, as the percentage cell density of *ei24⁻* cells did not decrease upon etoposide treatment (electronic supplementary material, Fig. S5).

***ei24* is a DNA-damage response gene**

Since etoposide caused DNA-damage and induced *ei24* expression, we asked if *Ddei24* is a DNA-damage response gene. For this, we checked the expression of DNA double strand break (DSB) repair genes [*rad51*, *52* and *54* for homologous recombination (HR) and *ku70*, *ku80* and *dnapks* for non-homologous end joining (NHEJ)] in the wild type, wild type treated with etoposide, *ei24^{OE}* and *ei24⁻* cells (Fig. 8D). We observed elevated expression of repair genes like *Rad54*, *Ku70*, *Ku80* and *dnapks* in *ei24^{OE}* and etoposide treated *Ax2* cells while the expression was low in *ei24⁻* cells, which directly refers to the enhancement of DNA-damage repair mechanism in response to increased *ei24* levels.

Cell cycle analysis of *ei24* mutants both in the presence and absence of etoposide

To find if changes in the cell cycle phases were indicative of cell fate, we checked for the percentage of cells in each phase of the cell cycle in the *ei24* mutants and compared them to the wild type cells (Fig. 9A). From the earlier studies, it is known that cells from S-phase show a bias towards prestalk/stalk pathway while cells in G2/M phase show a bias towards prespore/spore pathway (Weeks and Weijer, 1994). In the *ei24⁻* mutant, we observed a decrease in the percentage of cells in the G2/M phase indicating a lower bias towards prespore pathway while there was an increase in the percentage of cells in the S-phase suggesting increased prestalk bias. In the *ei24^{OE}* cells, there was an increase in the G2/M phase cells and a decrease in S-phase cells suggesting a prespore bias (Fig. 9A). Thus, this data confirmed that in the absence of *ei24*, the cells showed a bias towards prestalk pathway resulting in stalky phenotype as well as increased prestalk gene expression.

We also analysed the cell cycle progression in different *ei24* mutants both in the presence and absence of etoposide (Fig. 9B). We observed a time-dependent effect of etoposide on the cell cycle. After 48 h with 40 $\mu\text{g ml}^{-1}$ etoposide treatment, *Ax2* cells in G2/M population increased from 29.68 ± 1.52 to 50.11 ± 6.82 % as compared to control (28.85 ± 2.04 to 37.76 ± 2.99 %) (Fig. 9B) and in *ei24^{OE}* cells, G2/M population increased significantly both in the untreated and treated cell populations (Fig. 9C). On the other hand, in case of *ei24⁻* cells, no considerable increase in G2/M population was observed upon etoposide treatment (Fig. 9D). It suggested that not only etoposide treatment but also overexpression of *ei24* caused G2/M cell cycle arrest, which possibly could be the reason for cell death. This correlation to cell death needs further inves-

tigations. Negligible effect of etoposide on *ei24* cells confirmed the *ei24* gene of *D. discoideum* to be an etoposide-induced gene.

Discussion

ei24 gene encodes a putative tumour suppressor and shows high expression in *p53*-expressing cells, which subsequently are removed by cell death. Recently, with the help of conditional *ei24* knockout mice, it was shown that EI24 is a component of basal autophagy pathway (Zhao *et al.*, 2012). In *C. elegans*, knockdown of *ei24* by siRNA resulted in the accumulation of degradation-defective autolysosomes (Tian *et al.*, 2010). It was also shown that *ei24* is a *p53*-target and a DNA-damage response gene involved in growth suppression or/and apoptosis/autophagy (Gu *et al.*, 2000; Tian *et al.*, 2010). In an attempt to understand the importance of *ei24* in *D. discoideum*, we presently describe the identification and characterization of EI24 encoded by *ei24* gene. In case of *D. discoideum*, we could not identify any *p53* gene but a gene *DDB_G0288895* has been referenced as *p53-like* in dictyBase. Our results showed *ei24* mRNA expression remained

unchanged in the *DDB_G0288895* overexpressing cells, thus we propose that EI24 may be functional even in the absence of *p53* that may or may not have a tumour suppressor role. Alternatively, *DDB_G0288895* has been wrongly annotated as a *p53-like* gene.

Loss of *ei24* results in severe developmental abnormalities in *D. discoideum*

DdEI24 is evolutionarily closer to plant than animal proteins. The partial localization to ER was also confirmed. We have characterized the EI24 in *D. discoideum* and showed its involvement in the regulation of aggregate-size, cell proliferation and DNA-damage repair (Fig. 10). It is localized in the dying cell population suggesting its involvement in stalk-cell differentiation and death. We show that *ei24* cells are defective in the aggregate-size determination that may have caused the formation of a large number of small-sized aggregates. In fact, the defect is not limited only to aggregate-size determination mechanism, as the mutants also showed defects in cell proliferation, development and differentiation of prespore and prestalk cells. Since development and prespore differentiation is largely dependent on cAMP signalling and was reduced in

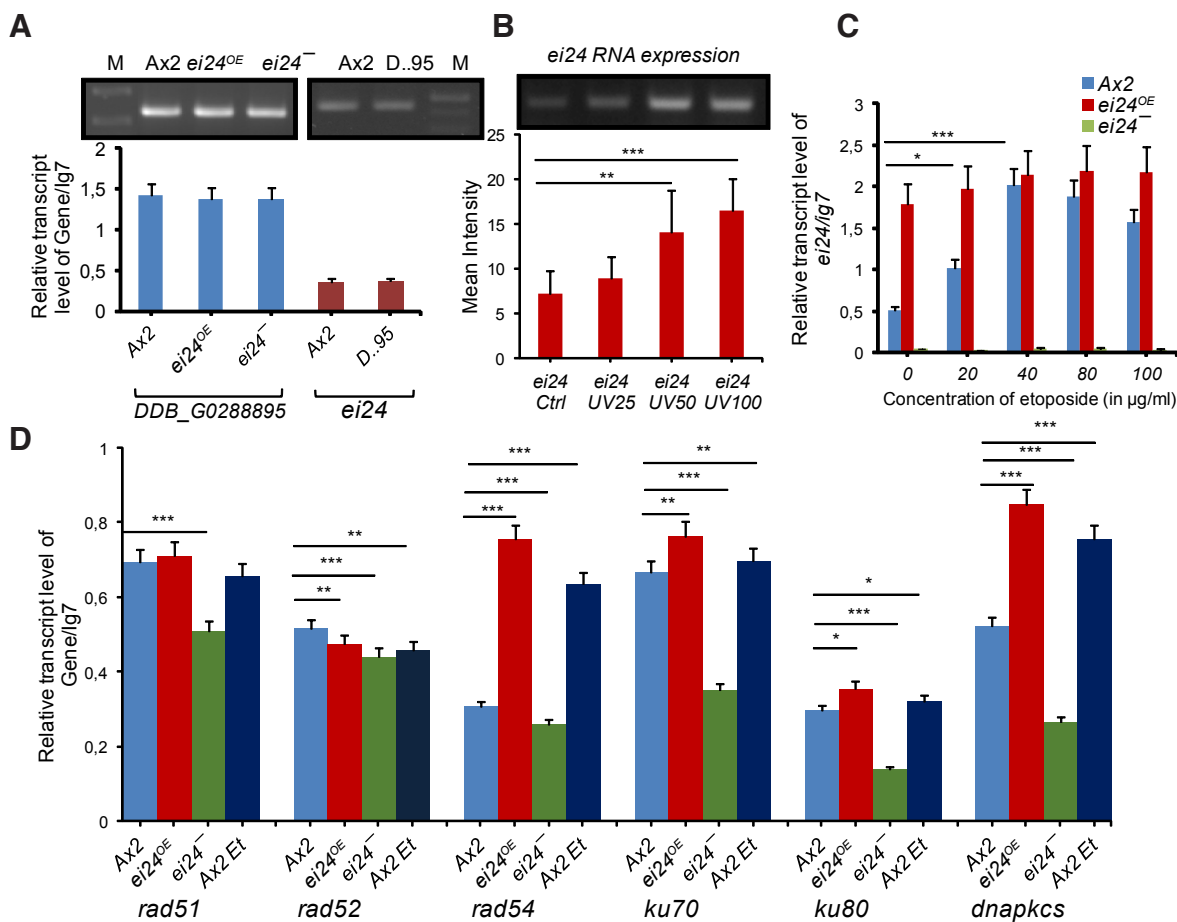


Fig. 8. *ei24* expression was induced in response to DNA-damage. (A) Bars represent relative *DDB_G0288895* (*p53*-like) expression that remained unchanged. Relative *ei24* expression remained unchanged in the *DDB_G0288895* overexpressing cells. Upper panel: one representative gel picture. (B) Graph shows induction of relative *ei24* expression with increasing dose of UV radiation (0–100 J cm⁻²). Upper panel: one representative gel picture. (C) Graph represents relative *ei24* expression that was induced in the wild type and *ei24*^{OE} cells but not in the *ei24*⁻ cells upon etoposide treatment (0–100 µg ml⁻¹). (D) Bar diagram shows relative mRNA expression levels of the repair genes *rad51*, *rad52*, *rad54* (HR) and *ku70*, *ku80*, *dnapkcs* (NHEJ) in wild type and *ei24* mutants. The wild type cells served as controls for both in presence and absence of 40 µg ml⁻¹ etoposide. [The values representing mean ± S.E.; n=3; Student *t*-test, *p*-value ≤0.05, ≤0.01 and ≤0.001 has been represented as *, **, and ***, respectively].

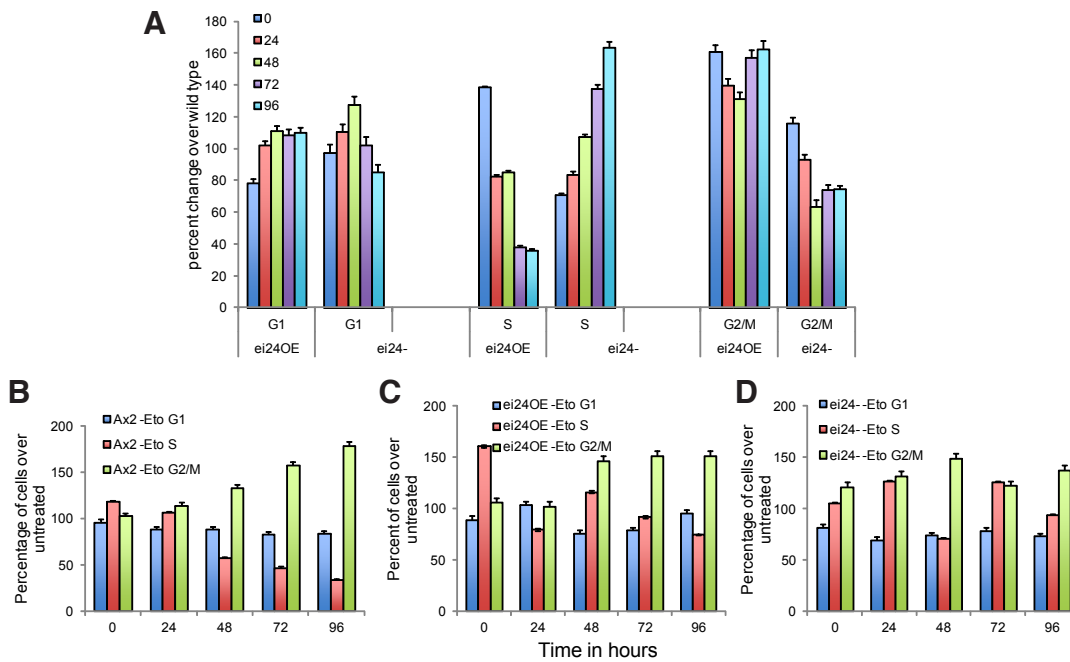


Fig. 9. Cell cycle analyses in the presence and absence of etoposide. Cell cycle analysis of wild type, *ei24^{OE}* and *ei24⁻* cells before and after etoposide ($40 \mu\text{g ml}^{-1}$) treatment at different time points (0 h, 24 h, 48 h, 72 h and 96 h) are shown. Percentage of cells in different phases of cell cycle was analysed by FACS. **(A)** Bardigrams show the percentage of cells over the wild type in G1, S and G2/M phases of the cell cycle in *ei24^{OE}* and *ei24⁻* cells at different time points. **(B-D)** Percentage of cells in each phase of the cell cycle at various time points after treatment with etoposide. The data represents the relative percentage of cells in each phase after normalizing to untreated samples of the same time for **(B)** Ax2; **(C)** *ei24^{OE}*; **(D)** *ei24⁻* strains. [The values representing mean \pm S.E.; $n=3$; Student *t*-test].

the *ei24⁻* cells, it could be the possible reason for the observed phenotype. The *vice-versa* could be observed with the *ei24^{OE}* cells. The phenotype observed by the *ei24⁻* cells could be also attributed to the cell-adhesion molecule and Countin factor. The expression of *countinA* mRNA was significantly increased in *ei24⁻* cells. Countin protein causes the aggregation streams to break-up resulting in small-sized aggregates and ultimately small-sized fruiting bodies. The *ei24⁻* cells showed increased *countin A* expression, which exhibits aberrant cell-adhesion to maintain the group-size. From our studies, we conclude that in wild type cells, EI24 represses Countin and subsequently cell-adhesion proteins to regulate the aggregate-size. It is possible that in the background of reduced cAMP levels, the amoebae chemotax feebly; therefore they tend to form small-sized aggregates due to increased cell-adhesion (*cadA*). The aggregates were small and did not require further break-up and thus showed reduced *csA* expression. This was confirmed by the feeble chemotaxis shown by *ei24⁻* cells.

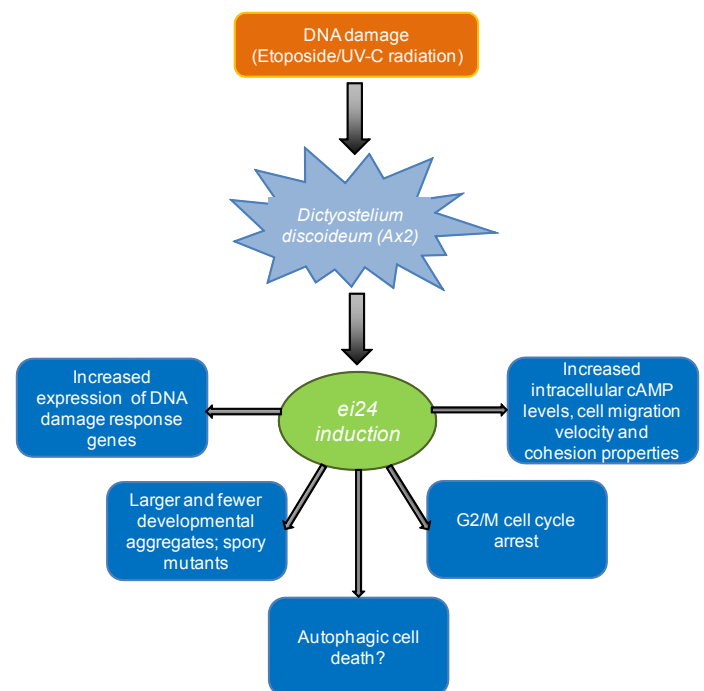
If localization has anything to do with the function we would expect *ei24* to be involved in prestalk/stalk differentiation. In the absence of *ei24*, we found stalky phenotype, mis-expression of prestalk genes and reduced cAMP signalling. All these suggest that in case of *Dictyostelium*, EI24 is involved in the cell-type proportioning. Cell cycle analyses also confirmed the cell-type bias by the mutants. Also, treatment of Ax2 cells with etoposide promoted G2/M arrest in cell cycle. Since treatment with etoposide showed a positive correlation with *ei24* expression, we also found G2/M arrest in the *ei24^{OE}* cells.

Fig. 10. Role of *ei24* in *D. discoideum* is schematically illustrated. *ei24* in *Dictyostelium* is induced upon DNA-damage either through UV-C irradiation or etoposide treatment. *ei24* caused formation of larger and fewer aggregates leading to spory fruiting bodies which are mainly due to increased intracellular cAMP levels, cell migration velocity and cell-cohesion properties. Induced *ei24* expression also caused G2/M cell cycle arrest protecting *ei24⁻* cells from DNA-damaging agents like etoposide. It also has a role in DNA-damage repair by increasing DSB repair gene expression. Its role in autophagic cell death is yet to be elucidated.

Our results showed that EI24 is not *p53*-like regulated gene *per se* rather it may serve as a sensor of cell death probably by autophagy induction. In our case, we observed overexpression did not negatively control cell proliferation but upon treatment with etoposide, death was observed. It is possible that it may not act as a tumour suppressor but may be an autophagy gene, which still needs to be confirmed.

Loss of *ei24* in *Dictyostelium* confers resistance to etoposide

Presently, we show the induction of *ei24* upon treatment with DNA-damaging agents like etoposide and UV radiation. Etoposide stabilizes a covalent complex between DNA topoisomerase II and



DNA resulting in the form of DSBs (Montecucco and Biamonti, 2007; Sung *et al.*, 2013). Repair of DNA-DSBs is critical for the maintenance of genome integrity and is repaired by either HR or NHEJ. We show that the DSBs caused by etoposide treatment of Ax2 cells or in *ei24^{OE}* cells could be repaired by HR and NHEJ pathway where NHEJ contributed more. It is established that the majority of vegetative *Dictyostelium* cells are present in the G2 phase of cell cycle and support HR mechanism, thus making HR the predominant pathway (Branzei and Foiani, 2008; Beucher *et al.*, 2009) but NHEJ must be functioning in some respect to combat DSBs during vegetative phase. Therefore, both HR and NHEJ are capable of repairing DSBs in *Dictyostelium*. Hsu *et al.*, (2011) have shown the requirement of Ku80 in the maintenance of G2/M arrest as the null cells could cross this checkpoint with persistent DSBs that are resolved in the subsequent cell cycle and facilitates DSB repair. Consistent with this, we too found that increased expression of *ei24* (*ei24^{OE}* or etoposide treatment) could elevate the levels of DSB repair genes. Taken together, this study exemplify that both NHEJ and HR are active in *Dictyostelium* and NHEJ plays a major role during *ei24* overexpression.

In conclusion, it will be important to determine if *ei24* is an autophagy gene as such studies would generalize the importance of EI24 beyond the actions of etoposide alone and could serve to point the function during autophagic pathway.

Materials and Methods

Homology search and phylogenetic analyses

The genomic DNA, cDNA and protein sequences of the EI24 family protein were obtained from dictyBase (www.dictybase.org/). To create a phylogenetic tree, amino acid sequences of approximately 20 different organisms ranging from prokaryotes to eukaryotes were aligned using the PHYLIP package. Sequences with insignificant branch support were removed manually and the neighbour-joining (NJ) tree formed was rooted on human EI24 and visualized in Newick format using MEGA6.0. program (Tamura *et al.*, 2013).

Growth and development of *D. discoideum*

Dictyostelium cells were grown axenically and cell proliferation was monitored according to Mishra *et al.*, (2017). Briefly, the logarithmic phase cells ($3\text{--}5 \times 10^6$ cells ml⁻¹) were used for inoculating the secondary culture at a starting density of approximately 5×10^5 cells ml⁻¹ and monitored over several days. Development analyses were performed according to Maurya *et al.*, (2017). The logarithmic phase cells were harvested, washed in $1 \times \text{KK}_2$ buffer and spotted at a density of 5×10^7 cells ml⁻¹ on non-nutrient agar (NNA) plates. The plated cells were synchronized for development at 4°C for 4–6 h, followed by incubation at 22°C. Analyses of developing structures were performed using NIS Elements AR v. 4.0.

RNA expression analysis

Spatiotemporal mRNA expression during development was analyzed using RT-PCR and *in situ* hybridization (Gosain *et al.*, 2012). mRNA levels were checked by gene-specific RT-PCR analysis and represented as relative to the internal control *mlA* (also called as *ig7*) transcript level.

The spatial mRNA expression in multicellular structures developed was investigated using *in vitro* transcription of exonic region (0.269 kb) that was PCR amplified and cloned into pBSII SK+ (pBluescriptII phagemid) vector (Stratagene). The construct was restricted to yield template for antisense and sense probe synthesis by T3 and T7 RNA polymerases, respectively. *In situ* hybridization was carried out using the kit available from Roche as per the manufacturer's instructions. The list of primer pairs used in this study is given in the electronic supplementary material, Table S1.

Generation of mutant strains

ei24 overexpressor (*ei24^{OE}*): Full-length *ei24* (DDB_G0284253) was PCR amplified from the Ax2 genomic DNA (4-1201 bp) using specific primers (Table S1) and cloned into *act15/acg-eYFP* vector containing the *actin15* promoter, reporter enhanced yellow fluorescent protein (eYFP) at the C-terminus, a G418 resistance marker for selection in *Dictyostelium* and an ampicillin resistance marker for selection in bacteria (electronic supplementary material, Fig S2A, upper panel). Positive constructs were then transformed into Ax2 cells and selected at 40 µg ml⁻¹ of G418 (Thermo-Scientific). Full-length *p53-like* (DDB_G0288895) gene was also expressed in Ax2 cells in a similar manner (electronic supplementary material, Fig S2A, lower panel).

ei24 knockout (*ei24⁻*): 5' (585 bp) and 3' (616 bp) *ei24* homologous fragments were amplified using specific primers and cloned flanking Blasticidin S resistance (Bsr) cassette in the pDrive vector (Maurya *et al.*, 2017). The resulting plasmid was digested with BamH1 and Not1 and the linearized gene-targeting construct was transformed into Ax2 cells. The transformants were selected on 10 µg ml⁻¹ Blasticidin S (Invitrogen) and independent clones were screened for the *ei24* deletion by PCR and RT-PCR (electronic supplementary material, Fig. S2B, C). *ei24* rescue strain (*ei24^{res}*): The overexpressing construct was transformed into *ei24⁻* cells and transformants were selected on both G418 and Blasticidin S.

Treatment with etoposide and UV radiation

The logarithmic phase cells (Ax2, *ei24^{OE}* and *ei24⁻*) were cultured in the absence and presence of etoposide (40 µg ml⁻¹, Sigma-Aldrich) for 48 h at 22°C. Relative transcript levels of *ei24* were compared. Similarly, log phase cells were exposed to different doses (0, 25, 50, 100 J m⁻²) of UV radiation (254 nm; Hoefer UV-C 500 crosslinker). Mean intensity of the cells was then measured using confocal microscopy (Andor Spinning Disc).

MTT assay

MTT (3-[4, 5-Dimethylthiazol-2-yl]-2,5-diphenyltetrazolium bromide) reduction assay was performed according to Swer *et al.*, (2014) to monitor cell viability upon treatment with etoposide.

Cell cycle analysis by flow cytometry

This was performed using FACS Calibur (Becton Dickinson, USA) according to Swer *et al.*, (2014) both in the presence and absence of etoposide. Briefly, 1×10^7 cells were fixed for 30 min at 22°C by adding chilled 75% ethanol drop-wise and incubated at 37°C for 30 min in the presence of 10 mg ml⁻¹ RNase A (Sigma-Aldrich) followed by further incubation at room temperature with 50 mg ml⁻¹ propidium iodide (Sigma-Aldrich). Cell Quest software for acquisition and analysis was used.

Spore-viability assay

This was performed according to Maurya *et al.*, (2017). Aliquots of 100 spores were mixed with a suspension of bacteria (*K. aerogenes*) and grown on SM agar plates for 5 days. The percent viability of spores was measured by counting the number of clear plaques formed on the bacterial lawns divided by total spores plated, followed by multiplication with 100.

Cell-cohesion assay

This was performed according to Mishra *et al.*, (2017). Briefly, logarithmic phase cells were developed for 4 h and cell aggregates formed were dispersed by vortexing and further re-suspended in $1 \times \text{KK}_2$ at a density of 2.5×10^6 cells ml⁻¹. They were allowed to re-aggregate on a platform shaker rotating at 180 rpm at 22°C. The number of non-aggregating cells (singlets and doublets) and clumped cells were counted and percentage of cell aggregation was calculated by dividing the difference of the total number of cells and the number of singlets and doublets by the total number of cells.

Chemotactic cell-migration assay

Briefly, 2×10^7 cells in $1 \times \text{KK}_2$ buffer were collected and allowed to develop

under shaken conditions for 6 h. Cells were re-suspended at a density of 1×10^6 cells ml^{-1} and placed ~5 mm away from the well filled with cAMP (5 μl cAMP; 100 μM) and further incubated for 1 h at room temperature under dark conditions (Mishra *et al.*, 2017). Cell movement in response to cAMP was captured with time-lapse images at 15 s per frame for 60 frames, using a Nikon TiE microscope. Cell migration ($\mu\text{m s}^{-1}$) was measured by ImageJ software.

cAMP concentration measurement

Total cAMP levels were measured using cAMP Enzyme Immunoassay Kit (CA200, SigmaAldrich). 1×10^6 cells from logarithmic phase culture of Ax2 and *ei24* mutants were starved in $1 \times \text{KK}_2$ buffer for 0, 4 and 6 h. Cells were harvested and treated with 0.1 M HCl. The cAMP assay was performed as per the manufacturer's instructions.

β -Galactosidase staining

β -Galactosidase staining in multicellular structures formed was performed according to Gosain *et al.*, (2012). Images were captured using a Nikon AZ100 microscope.

Statistical analysis

The statistical analyses were performed (mean standard deviation and standard error) and values were plotted in graph using Microsoft Excel-2013. Levels of significance were calculated using Student's t-test and p-values of less than 0.05 were considered as significant.

Acknowledgements

We gratefully acknowledge Mrs Tripti Panwar and Dr. Sarika Gupta from the CIF-SLS for their assistance in imaging and FACS, respectively.

Fundings

Partial Institutional funding (DST-PURSE, UGC-Networking, FIST-II, UPE-II) to SS are acknowledged. NG thanks ICMR for senior research fellowship.

References

- ALBRECHTSEN N, DORNREITER I, GROSSE F, KIM E, WIESMÜLLER L, DEPERT W (1999). Maintenance of genomic integrity by p53: complementary roles for activated and non-activated p53. *Oncogene* 18: 7706-7717.
- BALINT-KURTI P, GINSBURG G, RIVERO-LEZCANO O, KIMMEL AR (1997). rZIP, a RING-leucine zipper protein that regulates cell fate determination during *Dictyostelium* development. *Development* 124: 1203-1213.
- BEUCHER A, BIRRAUX J, TCHOUANDONG L, BARTON O, SHIBATA A, CONRAD S, GOODARZI AA, KREMPLER A, JEGGO PA, LÖBRICH M (2009). ATM and Artemis promote homologous recombination of radiation-induced DNA double-strand breaks in G2. *EMBO J* 28: 3413-3427.
- BRANZEI D, FOIANI M (2008). Regulation of DNA repair throughout the cell cycle. *Nat Rev Mol Cell Biol* 9: 297-308.
- BROCK DA, GOMER RH (1999). A cell-counting factor regulating structure-size in *Dictyostelium*. *Genes Dev* 13: 1960-1969.
- CHUNG CY, REDDY TB, ZHOU K, FIRTEL RA (1998). A novel, putative MEK kinase controls developmental timing and spatial patterning in *Dictyostelium* and is regulated by ubiquitin-mediated protein degradation. *Genes Dev* 12: 3564-3578.
- DASIKA GK, LIN SC, ZHAO S, SUNG P, TOMKINSON A, LEE EY (1999). DNA damage-induced cell cycle checkpoints and DNA strand break repair in development and tumorigenesis. *Oncogene* 18: 7883-7899.
- DEVKOTAS, JEONG H, KIM Y, ALI M, ROH J, HWANG D, LEE HW (2016). Functional characterization of *Ei24*-induced autophagy in the degradation of RING-domain E3 ligases. *Autophagy* 12: 2038-2053.
- EARLY AE, GASKELL MJ, TRAYNOR D, WILLIAMS JG (1993). Two distinct populations of prestalk cells within the tip of the migratory *Dictyostelium* slug with differing fates at culmination. *Development* 118: 353-362.
- GINSBURG GT, KIMMEL AR (1997). Autonomous and non-autonomous regulation of axis formation by antagonistic signalling via 7-span cAMP receptors and GSK3 in *Dictyostelium*. *Genes Dev* 11: 2112-2123.
- GOSAIN A, LOHIA R, SHRIVASTAVA A, SARAN S (2012). Identification and characterization of peptide: N-glycanase from *Dictyostelium discoideum*. *BMC Biochem* 8: 13-19.
- GU Z, GILBERT DJ, VALENTINE VA, JENKINS NA, COPELAND NG, ZAMBETTI GP (2000). The p53-inducible gene *Ei24/PIG8* localizes to human chromosome 11q23 and the proximal region of mouse chromosome 9. *Cytogenet Cell Genet* 89: 230-233.
- GU Z, FLEMINGTON C, CHITTENDENT, ZAMBETTI GP (2000). *ei24*, a p53-response gene involved in growth suppression and apoptosis. *Mol Cell Biol* 20: 233-241.
- HAN Z, FIRTEL RA (1998). The homeobox-containing gene *Warai* regulates anterior-posterior patterning and cell-type homeostasis in *Dictyostelium*. *Development* 125: 313-325.
- HSU DW, KIELY R, COUTO CA, WANG HY, HUDSON JJ, BORER C, PEARS CJ, LAKIN ND (2011). DNA double-strand break repair pathway choice in *Dictyostelium*. *J Cell Sci* 124: 1655-1663.
- JANG W, CHIEM B, GOMER RH (2002). A secreted cell number counting factor represses intracellular glucose levels to regulate group-size in *Dictyostelium*. *J Biol Chem* 277: 39202-39208.
- JANG W, GOMER RH (2008). Combining experiments and modelling to understand size-regulation in *Dictyostelium discoideum*. *J R Soc Interface* 5: S49-S58.
- LEHAR SM, NACHT M, JACKS T, VATER CA, CHITTENDEN T, GUILD BC (1996). Identification and cloning of *Ei24*, a gene induced by p53 in etoposide-treated cells. *Oncogene* 12: 1181-1187.
- MAURYAR, KUMAR R, SARAN S (2017). *Dictyostelium* AMPK α regulates aggregate-size and cell-type patterning. *Open Biol* 7: 170055.
- MONTECUCCO A, BIAMONTI G (2007). Cellular response to etoposide treatment. *Cancer Lett.* 252: 9-18.
- MISHRA H, BHADORIYA P, SARAN S (2017). Disruption of homeobox-containing gene, *hbx9* results in the deregulation of prestalk-cell patterning in *Dictyostelium discoideum*. *Differentiation* 94: 27-36.
- SUNG YH, JIN Y, KANG Y, DEVKOTA S, LEE J, ROH JI, LEE HW (2013) *Ei24*, a novel E2F target gene, affects p53-independent cell death upon ultraviolet C irradiation. *J Biol Chem* 288: 31261-31267.
- SWER PB, LOHIA R, SARAN S (2014). Analysis of rapamycin induced autophagy in *Dictyostelium discoideum*. *Indian J Exp Biol* 52: 295-304.
- SWER PB, BHADORIYA P, SARAN S (2014). Analysis of Rheb in the cellular slime mold *Dictyostelium discoideum*: cellular localization, spatial expression and overexpression. *J Biosci* 39: 75-84.
- TAMURA K, STECHER G, PETERSON D, FILIPSKI A, KUMAR S (2013). MEGA6: Molecular Evolutionary Genetics Analysis version 6.0. *Mol Biol Evol* 30: 2725-2729.
- TIAN Y, LI Z, HU W, REN H, TIAN E, ZHAO Y, LU Q, HUANG X, YANG P, LI X, WANG X, KOVÁCS AL, YU L, ZHANG H (2010). *C. elegans* screen identifies autophagy genes specific to multicellular organisms. *Cell* 141: 1042-1055.
- WEEKS G, WEIJER CJ (1994). The *Dictyostelium* cell cycle and its relationship to differentiation. *FEMS Microbiol Lett.* 124:123-130.
- WHITTINGHAM WF, RAPER KB (1960). Non-viability of stalk cells in *Dictyostelium*. *Proc Natl Acad Sci USA.* 46: 642-649.
- YANG J, BOGNI A, SCHUETZ EG, RATAIN M, DOLAN ME, MCLEOD H, GONG L, THORN C, RELLING MV, KLEIN TE, ALTMAN RB (2009). Etoposide pathway. *Pharmacogenet Genomics* 9: 552-553.
- ZHAO YG, ZHAO H, MIAO L, WANG L, SUN F, ZHANG H (2012). The p53-induced gene *Ei24* is an essential component of the basal autophagy pathway. *J Biol Chem* 287: 42053-42063.

Further Related Reading, published previously in the *Int. J. Dev. Biol.*

Dictyostelium discoideum Sir2D modulates cell-type specific gene expression and is involved in autophagy

Rakhee Lohia, Punita Jain, Mukul Jain, Pradeep Kumar Burma, Anju Shrivastava and Shweta Saran

Int. J. Dev. Biol. (2017) 61: 95-104

<https://doi.org/10.1387/ijdb.160038ss>

Cloning, expression and characterization of the ornithine decarboxylase gene from Dictyostelium discoideum

Rishikesh Kumar, Sheikh Rafia and Shweta Saran

Int. J. Dev. Biol. (2014) 58: 669-676

<https://doi.org/10.1387/ijdb.140174ss>

The Dictyostelium prestalk inducer DIF-1 directs phosphorylation of a bZIP transcription factor

Yoko Yamada, Yuzuru Kubohara, Haruhisa Kikuchi, Yoshiteru Oshima, Hong-Yu Wang, Susan Ross and Jeffrey G. Williams

Int. J. Dev. Biol. (2013) 57: 375-381

<https://doi.org/10.1387/ijdb.130046jw>

An orthologue of the Myelin-gene Regulatory Transcription Factor regulates Dictyostelium prestalk differentiation

Hiroshi Senoo, Hong-Yu Wang, Tsuyoshi Araki, Jeffrey G. Williams and Masashi Fukuzawa

Int. J. Dev. Biol. (2012) 56: 325-334

<https://doi.org/10.1387/ijdb.120030jw>

Synergy between two transcription factors directs gene expression in Dictyostelium tip-organiser cells

Hong Yu Wang and Jeffrey G. Williams

Int. J. Dev. Biol. (2010) 54: 1301-1307

<https://doi.org/10.1387/ijdb.103141hw>

Dictyostelium discoideum: a model system for differentiation and patterning

R Escalante and J J Vicente

Int. J. Dev. Biol. (2000) 44: 819-835

<http://www.intjdevbiol.com/web/paper/11206323>

Development at the edge of multi-cellularity: Dictyostelium discoideum

R R Kay

Int. J. Dev. Biol. (2000) 44: 35-38

<http://www.intjdevbiol.com/web/paper/10761844>



5 yr ISI Impact Factor (2016) = 2.421

